

Giorgio Ascenti, Achille Mileto, Bernhard Krauss,  
Silvio Mazziotti, Carmelo Sofia and Emanuele Scribano

---

### 3.1 Introduction

Renal masses are commonly detected during imaging of the kidneys. It has been estimated that over half of patients over the age of 50 years harbor at least one renal mass, most commonly a simple cyst. In particular, most of renal masses are discovered incidentally when an imaging examination is performed to evaluate a non-renal complaint. Although most represent benign renal cysts, not all incidental renal masses are benign, and most renal cell carcinoma (RCC) are also incidentally discovered in this scenario. Therefore, differentiating incidental benign renal masses from those that are potentially malignant is the most important challenge in daily practice [1–5].

RCC is the eight most common malignancy and according to estimates by the American Cancer Society, it was newly diagnosed in 64,000 people in the United States in 2012, and approximately 14,000 are expected to die of the disease [6].

The 2004 World Health Organization classification is now adopted and worldwide accepted for classification of renal tumors (Table 1). This classification distinguishes six types of renal tumors, based on histologic matrix arising (renal cell; metanephric; mixed mesenchymal and epithelial; nephroblastic, neuroendocrine; other origins). In particular, among renal cell tumors, benign and malignant are distinguished. Moreover, this classification lists inherited or familial predisposition (known inherited syndromes) to

renal neoplasms, which is present in less than 4 % of renal tumors [7].

Clear cell-type RCC is the most frequent variant, accounting to 80 % of all cases of renal tumors. Most clear cell RCC are solitary cortical neoplasms that occur with equal frequency in either kidney; multicentricity (4 %) and bilaterality (0.5–3.0 %) may be seen. Clear cell-type RCC has a worse prognosis compared with other histologic subtypes [8].

Papillary carcinoma, which accounts to 10 % of all renal cell carcinomas, has a less aggressive clinical course than RCC clear cell type. Papillary carcinoma has variable proportions of papillae and may be bilateral or multifocal with frequent hemorrhage, necrosis, and cystic degeneration. Cellular type 1 and type 2 tumors have been recognized with papillae covered by small cells with scanty cytoplasm arranged in a single layer in type 1, and tumor cells of higher nuclear grade, eosinophilic cytoplasm and pseudostratified nuclei in type 2 [7–9].

Multilocular cystic-type RCC is considered a specific entity in the current WHO classification [7], with an incidence ranging between 1 and 4 % of all renal tumors. Multilocular cystic RCC has excellent outcome and appears entirely composed of cysts of variable size, which are lined by a single layer of clear cells small papillae, and are separated from the kidney by a fibrous capsule.

Chromophobe-type RCC is less aggressive than other RCC types and accounts for 5 % of renal epithelial tumors. Some authors suggest a

**Table 1** WHO classification of renal tumors (modified from Ref. [7])

Familial renal cancer
<b>Renal cell tumors</b>
<i>Malignant</i>
Clear cell renal cell carcinoma
Multilocular clear cell renal cell carcinoma
Papillary renal cell carcinoma
Chromophobe renal cell carcinoma
Carcinoma of the collecting ducts of Bellini
Renal medullary carcinoma
Xp11 translocation carcinomas
Carcinoma associated with neuroblastoma
Mucinous tubular and spindle cell carcinoma
Renal cell carcinoma unclassified
<i>Benign</i>
Papillary adenoma
Oncocytoma
<b>Metanephric tumors</b>
Metanephric adenoma
Metanephric adenofibroma
Metanephric stromal tumors
<b>Mixed mesenchymal and epithelial tumors</b>
Cystic nephroma
Mixed epithelial and stromal tumor
Synovial sarcoma
<b>Nephroblastic tumors</b>
Nephrogenic rests
Nephroblastoma
Cystic partially differentiated nephroblastoma
<b>Neuroendocrine tumors</b>
Carcinoid
Neuroendocrine carcinoma
Primitive neuroectodermal tumor
Neuroblastoma
Phaeochromocytoma
<b>Other tumors</b>
Mesenchymal tumors
Hematopoietic and lymphoid tumors
Germ cell tumors
Metastatic tumors

relationship between chromophobe-type RCC and oncocytoma, with the foregoing which is thought to be the benign counterpart of chromophobe-type RCC [10]. Collecting duct and medullary-type RCC carcinoma accounts up to 2 % of all cases of renal tumors. While the collecting duct type derives from the “principal cells” of the collecting duct, medullary-type RCC is a rapidly growing rare tumor of the renal medulla. Several authors regard the medullary-type as an aggressive variant of the collecting duct-type RCC [11].

Oncocytoma and angiomyolipoma are the two most common benign lesions of the kidney.

Oncocytoma comprises 3–9 % of all primary renal neoplasms. Males are affected twice as often as females. Due to the absence of peculiar macroscopic imaging findings, lesions are challenging to distinguish from RCC. Renal angiomyolipomas (AML) are hamartomas composed of vascular, smooth muscle, and mature fat. The majority of angiomyolipomas are sporadic (80 %) and are typically identified in adults; the remaining 20 % are syndromic. They can usually have characteristic imaging appearances [9–12].

Besides these types of renal masses, common daily findings are benign renal cysts. The overwhelming majority of renal cysts are found by chance in the general population and are detected on US or CT in more than 50 % of patients older than 50 years [13]. Most renal cysts represent benign “leave alone” renal cortical lesions and require neither surgical resection nor follow-up imaging. Uncommonly, however, RCC can present as a complex cystic renal lesion and thus, it is mandatory to distinguish benign cysts from cystic RCC [14].

RCC, as in general most of renal masses, may remain clinically occult for most of its course. The classic triad of flank pain, hematuria, and flank mass is uncommon (10 %), and it is indicative of advanced disease in patients with RCC. Twenty-five to thirty percent of patients are asymptomatic, and their RCC are found on incidental urologic or abdominal imaging study [15].

### 3.2 State of the Art of Conventional (Multidetector) CT

MDCT is the mainstay in the characterization and staging of renal masses. When one is specifically asked to characterize a renal mass with CT, the examination needs to be performed before and after administration of intravenous contrast material [5, 13, 16].

Pre-contrast images are used for baseline density measurements in both solid and complex cystic masses but also provide information about morphological and structural features, such as the presence of intralosomal fat or calcium.

Post-contrast images are used to evaluate enhancement, defined as delta of CT density measured on pre- and post-contrast images. Although contrast-enhancement do not necessarily indicate malignancy of a renal mass, either solid (i.e., oncocytoma and angiomyolipoma with no macroscopic fat) either complex cystic (i.e., inflammatory cyst), it represents the diagnostic clue that permits to differentiate surgery-needing from non-surgery-needing renal masses.

After intravenous contrast material administration, three different phases of renal enhancement are acquired: the corticomedullary phase, in which there is corticomedullary differentiation and which occurs 20–70 s after the injection of contrast material; the nephrographic phase, in which there is a homogeneous maximally enhanced nephrogram and which occurs 80–120 s after the injection of contrast material; the excretory phase, in which the nephrogram is homogeneous, but there is decreased enhancement of the parenchyma because contrast material has been excreted into the collecting system and which occurs 5–10 min after the administration of contrast material (Fig. 3.1) [17, 18].

The nephrographic phase is ideal to detect and characterize renal masses. Because there is maximal and homogeneous parenchymal enhancement, this allows better detection of renal masses, which typically do not enhance to the same degree as the renal parenchyma. The corticomedullary and excretory phases

occasionally may make the detection of renal masses more difficult. During the corticomedullary phase, small renal masses may be indistinguishable from the renal medulla; during the excretory phase, renal masses may be of the same attenuation as the renal parenchyma, which has de-enhanced [17, 18].

During the nephrographic phase, most of renal neoplasms are maximally enhanced. Because the identification of enhancement is necessary to diagnose a neoplasm, maximal enhancement of neoplasms is especially important in the hypovascular ones (papillary RCC). In these cases, the unequivocal demonstration of enhancement is challenging because papillary renal cell carcinomas are particularly prone to enhance less and at a slower rate than other tumors [19]. Imaging in the corticomedullary phase is useful in showing the normal corticomedullary pattern in pseudotumors such as prominent columns of Bertin, as in depicting renal vasculature for a nephron-sparing surgery [20]. Furthermore, the typical hypervascular pattern of clear cell renal carcinoma can be demonstrated in this phase. Imaging in the excretory phases is required when an involvement of the excretory system is suspected [16–19].

When encountering any renal mass, it is necessary to first determine whether the detected abnormality represents a pseudotumor, a mass-like finding that mimics a neoplasm. Renal pseudotumors are caused by a variety of conditions including congenital anomalies (prominent renal column of Bertin, dromedary humps) (Fig. 3.2), inflammatory masses (focal pyelonephritis, chronic renal abscess, and autoimmune disease), vascular structures (renal artery aneurysm or arteriovenous fistula), or abnormalities relating to trauma or hemorrhage. Although some renal pseudotumors require treatment, they are treated differently from neoplasms, and therefore, their recognition is important to ensure proper management. If they are not first excluded when evaluating a renal mass-like finding, the application of image-based criteria used to evaluate renal masses could lead to an incorrect diagnosis. For example, enhancement

**Fig. 3.1** Example of different MDCT renal protocol study phases. Coronally reformatted unenhanced (a), corticomedullary (b), nephrographic (c), and excretory (d) phases

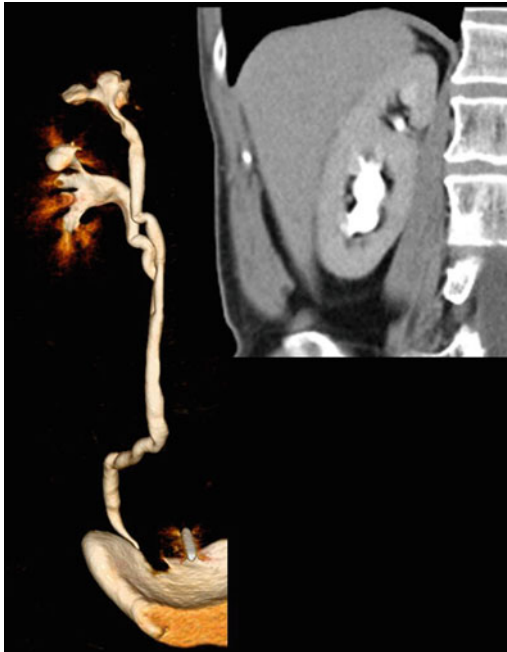
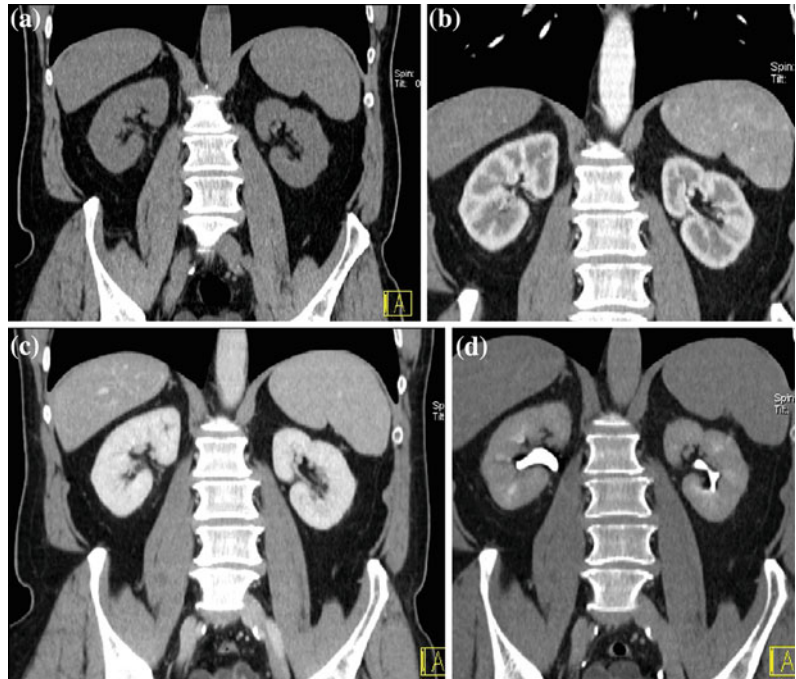
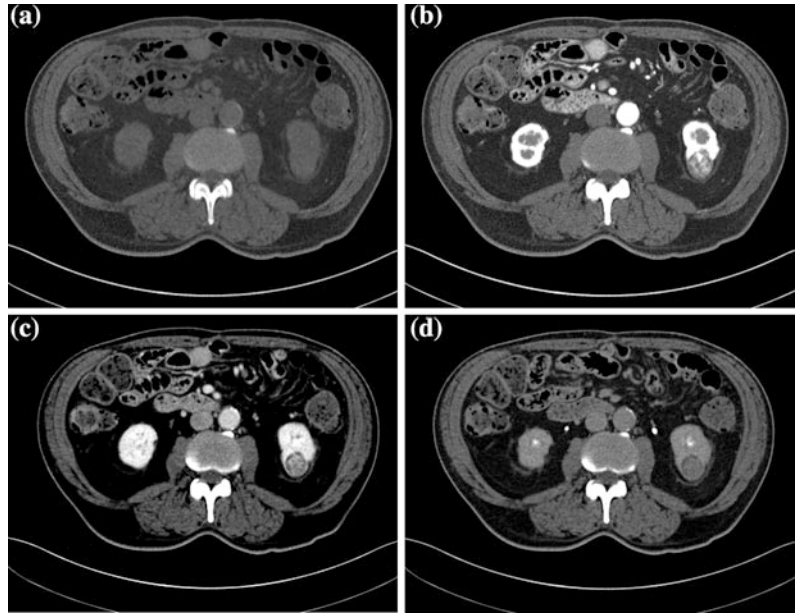


**Fig. 3.2** Volume-rendering and coronally reformatted nephrographic phase images in a patient with hypertrophic Bertin column associated with double collecting system

is often used to support the diagnosis of a neoplasm, but enhancement can be found in infectious and other inflammatory conditions, aneurysms, and vascular malformations. Key radiologic features to support an inflammatory cause include ill-defined margins and perinephric fat stranding. Aneurysms and vascular malformations enhance similar to nearby vasculature; in the case of a vascular malformation, hypertrophy of the ipsilateral renal artery and arteriovenous shunting may be present. Finally, in the presence of a renal pseudotumor, the same degree of enhancement respect to normal parenchyma in all study phases is the diagnostic clue [20].

Once pseudotumors are excluded, mass enhancement indicates a neoplasm (Fig. 3.3). Renal mass enhancement is affected by multiple factors: the amount and rate of the contrast material injected, scan delay, and the vascularity of the mass. Highly vascular tumors show marked enhancement, whereas hypovascular tumors show minimal enhancement. There is no universally agreed upon specific value that can

**Fig. 3.3** Unenhanced (a) and contrast-enhanced corticomedullary (b), nephrographic (c), excretory (d) study phases in a patient with RCC, clear cell type, of the left kidney



be used as a cutoff point for differentiating non-enhancing cysts from enhancing solid tumors. In MDCT, a threshold of 20 HU is worldwide used to indicate definitive enhancement within a renal mass, values of 10–19 HU as equivocal for enhancement, and values of less than 10 HU as indicating no enhancement [5, 20].

Cystic lesions are the most commonly detected renal masses, with most being benign simple cysts. Simple cysts are defined as having a hairline-thin wall, no septa or calcification, and being filled with simple fluid that measures 0–20 HU (Fig. 3.4). There are no soft-tissue components within simple cysts; they do not enhance after the administration of contrast medium, and they are considered benign [21–23]. When a cystic renal mass contains material showing attenuation higher than simple fluid (>20 HU), one or more septa, calcifications, thickened walls or septa, or enhancing soft-tissue components, it cannot be considered a simple cyst. The Bosniak classification system has been used worldwide in evaluating cystic renal masses over the past 25 years. Cystic renal masses are classified into 5 groups based on CT findings: categories I, II, IIF, III, and IV [22, 24–26]. Category I masses are simple cysts and are

always benign. Category II masses are minimally complicated cysts that can be reliably considered as benign. They may contain a few (generally 1 or 2) hairline-thin septa in which perceived (not measurable) enhancement may be appreciated. The wall or septa may contain fine calcifications or a short segment of slightly thickened smooth calcification. High-attenuation cysts  $\leq 3$  cm are also included in category II (Fig. 3.5). These masses were initially described as containing attenuation higher than renal parenchyma (typically 40–90 HU), but the attenuation criterion has been expanded to include masses with attenuations more than 20 HU. To diagnose a high-attenuation cyst, the mass must be well circumscribed, homogeneously high-attenuating and must not enhance. Homogeneity is an important feature; high-attenuation fluid within a renal mass may mask small regions of enhancement. Therefore, it is important to obtain multiple attenuation measurements of varying sizes throughout the lesion to ensure that the mass is homogeneous and that no portion of the mass enhances [20, 22, 25, 27].

Category IIF lesions are likely benign but require follow-up imaging to show stability. These masses may contain multiple hairline-thin

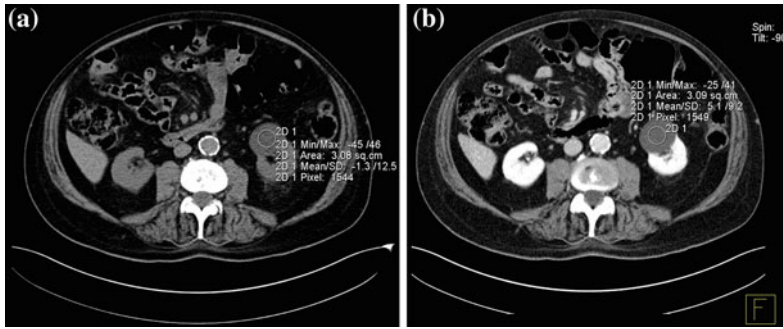


**Fig. 3.4** Axial unenhanced (a) and contrast-enhanced nephrographic (b) phase images in a patient with left renal simple cyst. The lesion shows baseline water

density (a) and no contrast-enhancement on nephrographic phase image is seen (b)

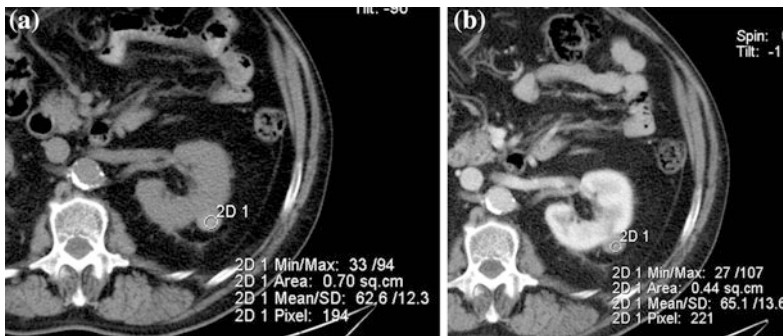


**Fig. 3.5** Axial unenhanced (a) and contrast-enhanced nephrographic (b) phase images in a patient with high-attenuation (Bosniak category II) cyst of the left kidney.

The lesion shows baseline high-density (a), consistent with hemorrhagic content, and no contrast-enhancement on nephrographic phase image is seen (b)

septa in which enhancement may be visually perceived (not measurable enhancement). Category IIF renal masses may contain thick or nodular calcification, with no soft tissue enhancing nodules. Non-enhancing high-attenuation renal cysts that measure more than 3 cm are included. Category IIF masses should be followed for morphologic and structural changes, such as development of septa, wall thickening, or new areas of enhancement, suggestive of malignancy. Growth is not a useful determinant of malignancy, because simple benign cysts may grow and renal cell carcinomas may not. Therefore, growth is not a feature of the Bosniak renal cyst classification [22–27]. The recommended interval for follow-up examinations is to obtain a CT scan or MR imaging examination at 6 and 12 months, followed by

yearly examinations for a minimum of 5 years. However, there is no known time interval of stability that can be used to diagnose a renal mass as benign with complete certainty. However, whether a Bosniak category IIF lesion has not significantly morphologically changed in a period of 5 years, it is likely benign [22].

Category III cysts are truly indeterminate masses because they have a reasonable probability of being benign or malignant. Imaging features include a thickened wall or septa that show measurable enhancement. Benign masses in this category include acute and chronically infected cysts, hemorrhagic cysts (often secondary to trauma), benign multiseptated cysts, and cystic neoplasms such as multilocular cystic nephroma. Malignant masses in this category include multilocular cystic RCC. Initially, it was

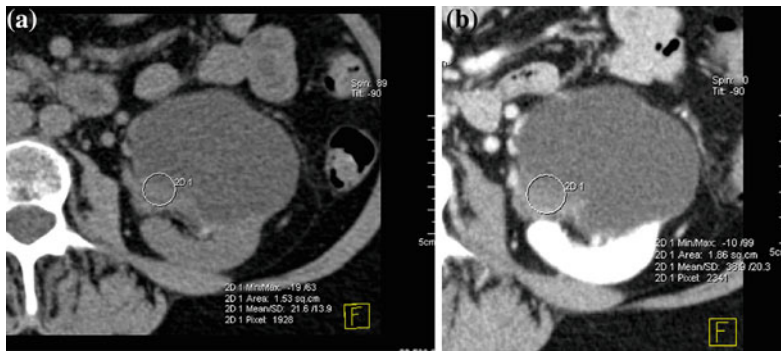


**Fig. 3.6** Axial unenhanced (a) and contrast-enhanced nephrographic phase (b) images in a patient with cystic RCC (Bosniak category IV). The lesion shows a mural

nodule with soft-tissue baseline density (a) that has moderate enhancement on nephrographic phase image (b)

estimated that approximately half of category III masses were benign and the other half were malignant. Recent studies have shown a wide range (31–100 %) of these masses to be malignant. This wide variation may be attributed either to radiologists' experience in renal mass imaging or to practice of referring urologists caring for the patient. Since category IIF was introduced, most category III renal masses that were previously removed are now being followed (category IIF), with a subsequent greater percentage of malignant category III masses remaining. Surgery remains the preferred treatment if the patient does not have high surgical risk [5, 22, 25].

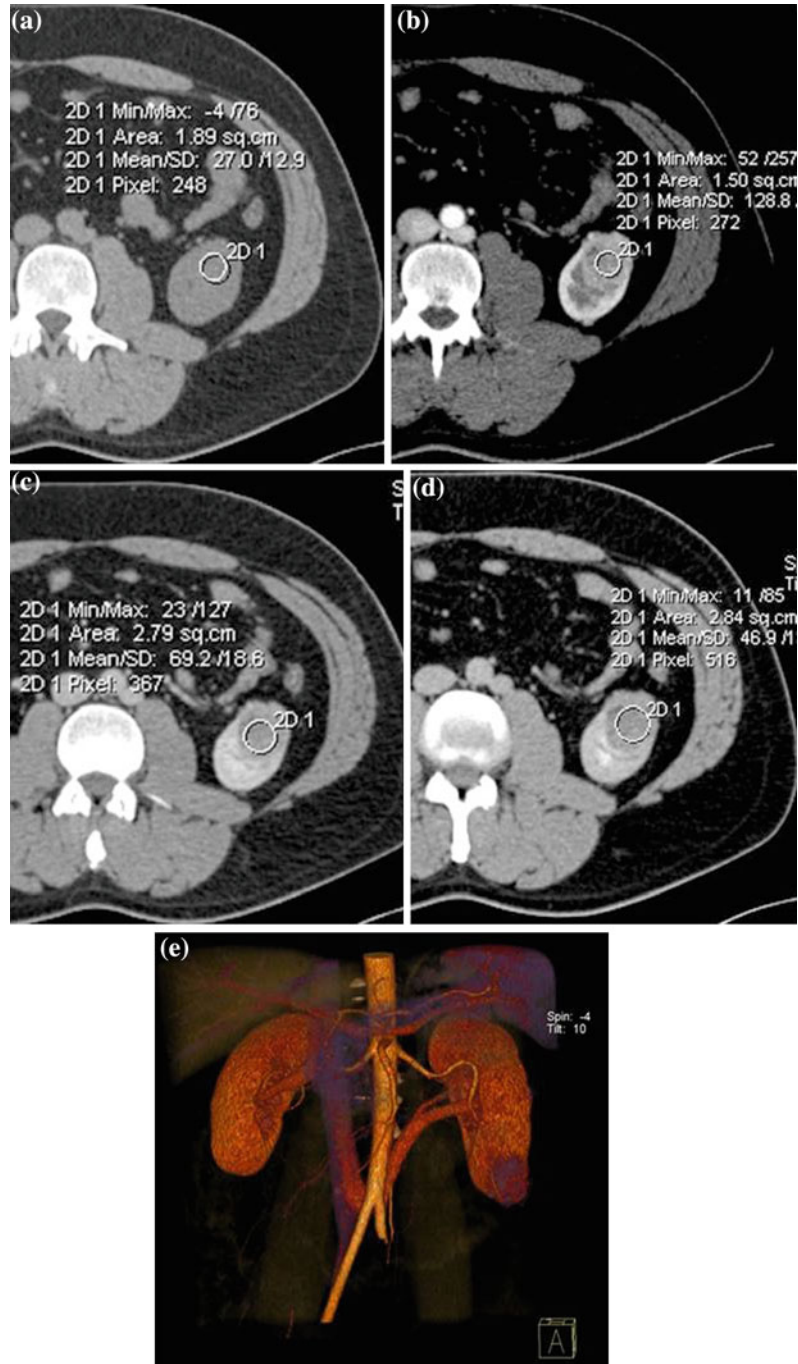
Finally, category IV cysts are clearly malignant masses until proved otherwise and therefore require surgical removal. Imaging features include those described in category III with the additional presence of nodular enhancement within the mass or adjacent to its wall (Fig. 3.6). The probability of such a mass being malignant is close to 100 % [22–30].

Although there are well-established, time-tested, image-based criteria, it is often very difficult distinguishing benign complicated from malignant cystic renal masses mainly due to the overlap between the gross morphologic and radiologic findings. Thus, characterization of complex cystic renal masses, as malignant

lesions requiring surgery and non-malignant lesions that do not, remains a common diagnostic challenge [28–30].

A solid renal mass is best defined as having little or no fluid components and usually consists predominantly of enhancing soft-tissue. As detailed earlier, after excluding pseudotumors, a solid renal mass should be considered a renal neoplasm. In particular, whether a solid renal mass enhances by more than 20 HU, or whether it shows enhancement in the simultaneous presence of calcification and macroscopic fat, it has to be considered as RCC until proven otherwise and pathology is mandatory (Fig. 3.7) [5, 17, 20]. It is also necessary to diagnose those malignant renal neoplasms that do not require surgery (e.g., lymphoma and metastatic disease). A combination of clinical history and imaging findings may allow these masses to be diagnosed. However, in some cases, percutaneous biopsy may be required. When there is a history of an extra-renal primary tumor, the 50–85 % of solitary renal masses are metastatic. Therefore, if a solid renal mass is detected in a patient with a known primary malignancy (e.g., lung cancer, lymphoma), a metastasis should not be necessarily diagnosed presumptively; both a second primary (RCC) and a benign neoplasm should be considered [5, 17, 20].

**Fig. 3.7** Axial unenhanced (a), contrast-enhanced corticomedullary (b), nephrographic (c) and excretory (d) study phases, with corresponding VR image (e) in a patient with RCC, clear cell type, of the left kidney. The lesion shows soft-tissue baseline density (a) and enhancement after contrast-medium administration (b, c). This nodule has moderate enhancement on nephrographic phase image (c) and progressively de-enhances on excretory phase image (d)



However, many small ( $\leq 3$  cm) solid renal masses are benign [31]. Benign diagnoses typically encountered at surgery, for what was previously believed to be RCC mainly include oncocytomas and angiomyolipomas.

Oncocytoma is a benign solid renal mass that cannot be differentiated from RCC by imaging. Although a central scar or homogeneous enhancement at CT or MRI is suggestive of oncocytoma, these findings are not specific and a



tissue diagnosis is necessary to differentiate oncocytoma from RCC [31–33].

Angiomyolipoma is a benign neoplasm that, particularly when small, warrants no treatment. Most angiomyolipomas can be diagnosed by identifying regions of fat within a non-calcified renal mass at unenhanced CT. Some angiomyolipomas contain very small quantities of fat that can be overlooked if the mass is not carefully evaluated. However, approximately 5 % of angiomyolipomas do not contain fat that can be seen at imaging, and the differentiation from other renal neoplasms is not possible with CT. These masses, referred to as angiomyolipoma with minimal fat, are often small, mildly hyperattenuating on unenhanced CT examination and homogeneously enhanced with contrast material. However, these findings are not specific enough to make a confident diagnosis of an angiomyolipoma, and other tumors, such as papillary RCC, metanephric adenoma, oncocytoma and leiomyoma, may have a similar appearance [34, 35].

Further problems in enhancement evaluation, mainly due to multiphasic acquisition, i.e., different positioning of region-of-interest (ROI) on sequential images or difficulty with appropriate placement of a ROI in intrarenal tumors that are isodense to parenchyma on unenhanced image, make sometimes a definitive diagnosis difficult at MDCT, especially when small hypovascular tumors are encountered. Another frequent problem is represented by the pseudoenhancement, which is defined as an artificial elevation of the HU attenuation of a simple renal cyst imaged on contrast-enhanced CT image during nephrographic phase, at peak of parenchymal enhancement. Pseudoenhancement is thought to be principally due to the image reconstruction algorithms used to adjust for beam-hardening artifacts [36, 37].

---

### 3.3 Spectral CT: Study Protocols and Clinical Applications

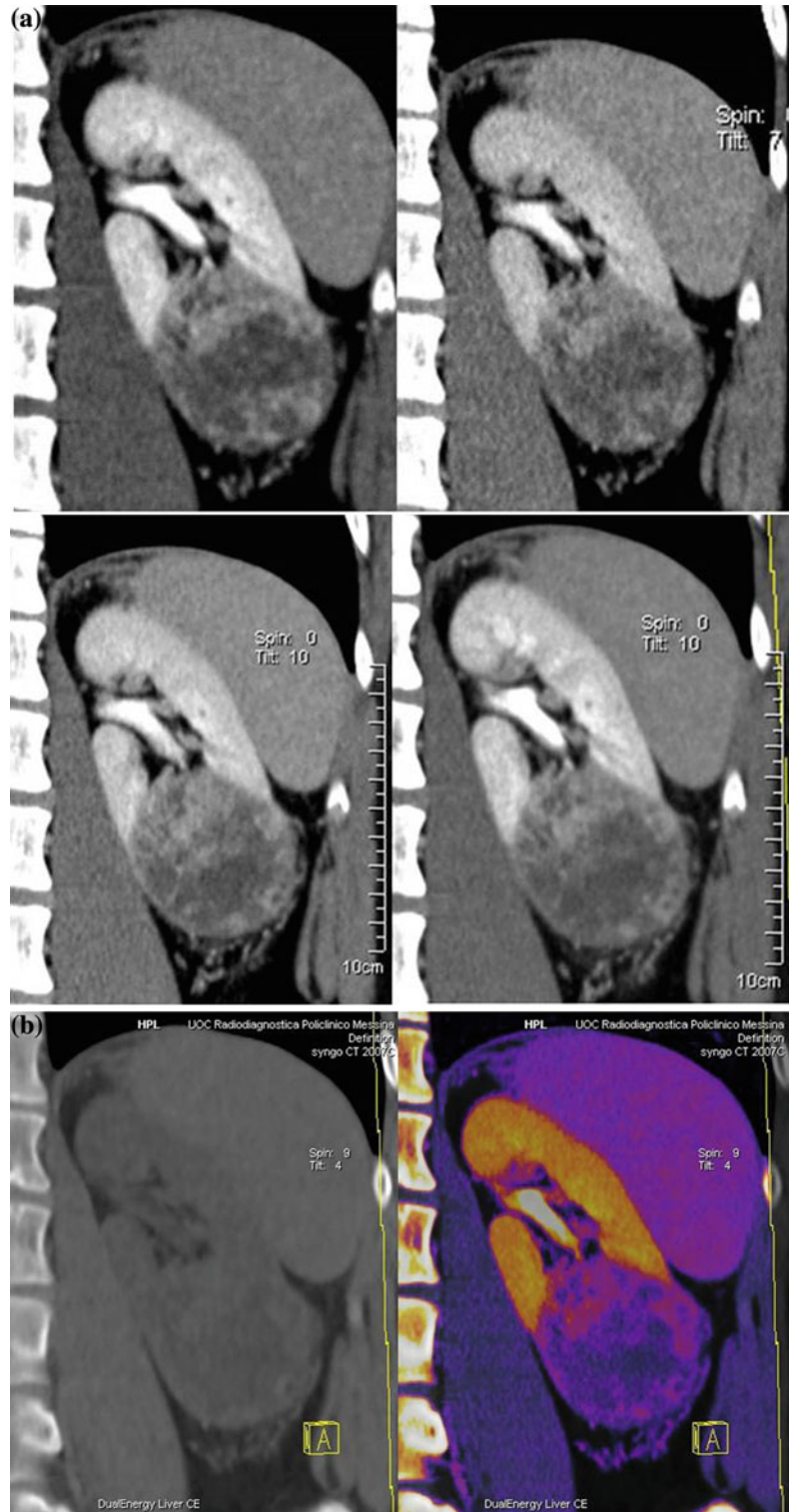
By means of spectral analysis, dual-energy imaging provide complementary information and approach toward a new hybrid, morphologic-functional imaging.

Various clinically relevant applications have been established for dual-energy CT renal lesion imaging [38–45]. These applications can be distinguished in *non-material-specific*, *material-specific*, and *energy-specific* (Fig. 3.8).

*Non-material-specific* applications permit to enhance the iodine image conspicuity while optimizing the contrast-to-noise ratio. The two datasets obtained from dual-energy acquisition at high and low kVp can be separately analyzed or blended in a single image stack. In particular, high-energy images have the advantage of lower noise scan, but at the same time, this advantage is offset by the decrease in contrast resolution. On the other hand, low-energy images show a better contrast resolution, but the acquired dataset is noisier (Fig. 3.8) [39–41].

Both to exploit benefits and to alleviate drawbacks of both kVp scans fused (140- and 80-kVp) datasets with an intermediate weighting and different blending strategies have been developed. The first used approach was a linear-blending fashion that uses a simple linear-blending algorithm using fixed percentages of 80- and 140-kVp datasets. Several studies, both in vitro and in vivo, demonstrated that a linear-blending ratio of 70 % 140-kVp and 30 % 80-kVp have image characteristics similar to a standard single-energy scan and thus can be considered a simulated weighted-average 120-kVp dataset (Fig. 3.8). On second-generation dual-source scanner, the linear-blending ratio of 50 % from 100-kVp and 50 % from 140-kVp datasets has image characteristics similar to a standard 120-kVp single-energy scan. However, the application of a fixed weighting factor for all pixels reduces both noise and high contrast [46–48]. The second strategy, alternative to linear blending, is represented by non-linear image-blending mode (Fig. 3.8). The goal of this mixing strategy is to maintain the contrast of the low-energy scan, while achieving the noise characteristics of the high-energy scan. In particular, the high-intensity regions corresponding to iodine contrast-enhancement are preferentially extracted by 80-kVp data, to maintain the high image contrast in regions of high iodine concentration. By contrast, low-intensity levels, which correspond to air, water, and soft tissues,

**Fig. 3.8** Dual-energy non-material-specific (a), material-specific (b) and energy-specific (c) applications in a patient with RCC, clear cell type, of the left kidney. The low-kVp (upper left corner) and high-kVp (upper right corner) can be separately analyzed (a) or blended in a single image stack in either a linear (lower left corner) or alternatively in a non-linear fashion (lower right corner). Based on a three-material decomposition algorithm (b) iodine spectral extraction image series is created, with virtual unenhanced (left) and color-coded iodine overlay image (right) series. By applying a mathematic computerized model to the polychromatic source data obtained from the dual-energy acquisition, separate monochromatic image series (c) are created



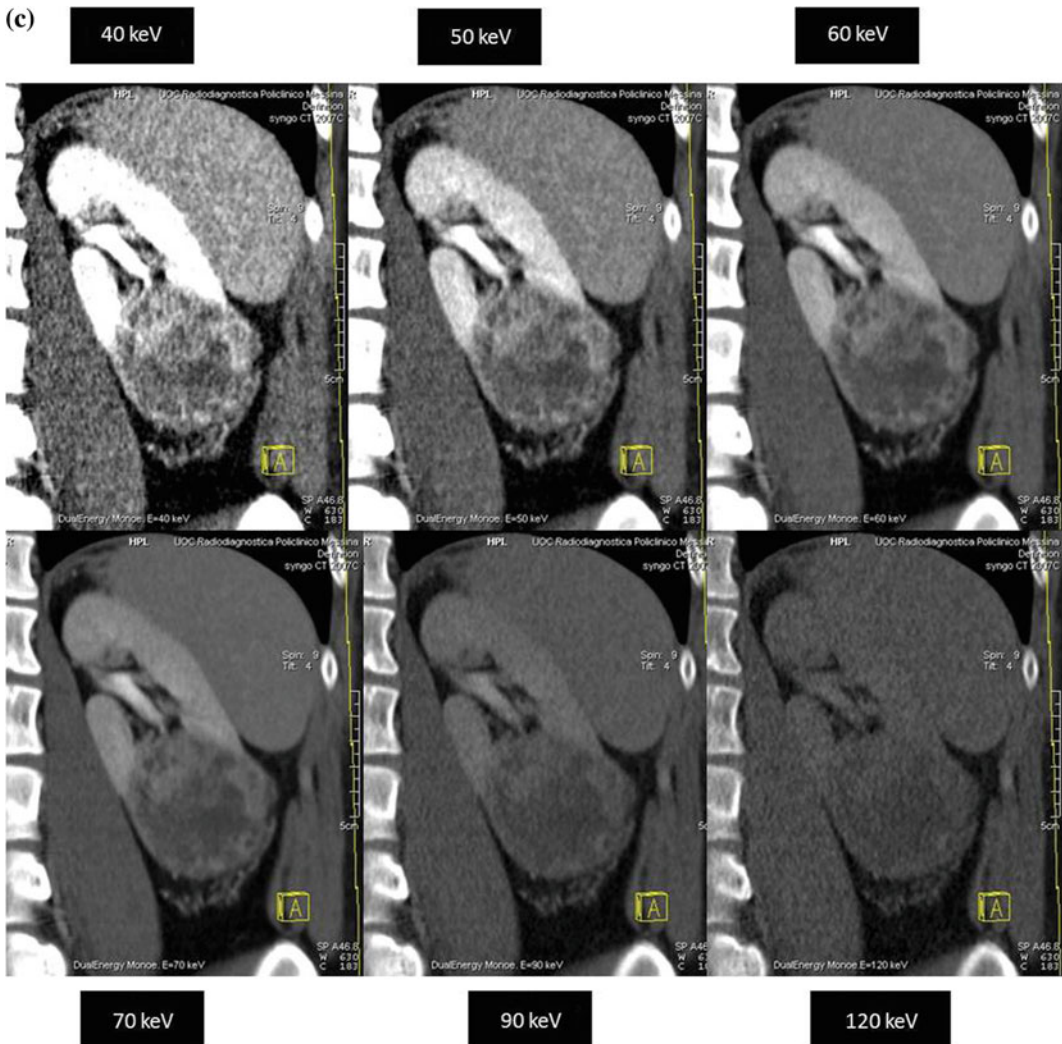


**Fig. 3.8** (continued)

are less noisy in 140-kV scan and should be preferred in the blending process [49, 50]. The result is an image in which iodine signal is magnified, while optimizing contrast differences and minimizing image noise. Several non-linear-blending functions including a binary-blending function, a slope blending function, a Gaussian function, and a modified sigmoid function have been developed. Recently, a piecewise linear-blending function method has been commercially implemented in the dual-source platform (labeled as “Optimum Contrast”). A recent study has demonstrated that,

compared with a standard linear-blending reconstruction algorithm, a piecewise linear-blending function method leads to significantly improve tumor conspicuity and enable better image quality in the evaluation of renal masses at DECT during nephrographic phase of enhancement [51]. This can be useful in defining neoplastic or inflammatory renal medullary pyramids infiltration and permits to reduce the flow rate and amount of administered contrast medium in patients with mild impairment of renal function.

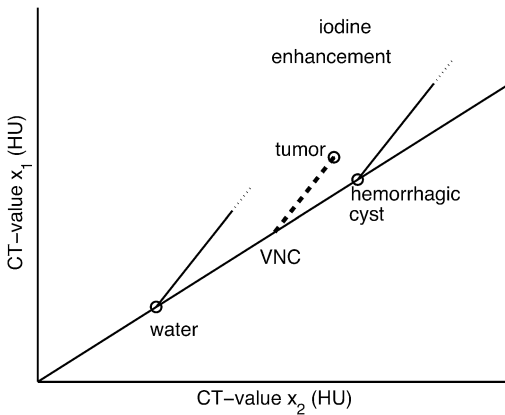


**Fig. 3.9** Drawing shows how material decomposition into iodine and water is used to calculate the iodine enhancement and virtual non-contrast images. Note that there is a simple parallel projection in the CT-value diagram

*Material-specific* applications, mainly based on three- or two-material-decomposition principles, allow the reader to differentiate, isolate and quantitate different materials having different  $k$ -edge values. This capability to extract materials improves as they show high atomic number (i.e., iodine or calcium) [39, 52, 53].

These applications are based on the fact that iodine enhancement is much higher at low tube voltage than at high tube voltage (typically a factor of 2 between 80 kV and 140 kV), whereas body soft tissues (with the exception of fat) have approximately the same CT values for both spectra. Therefore, in terms of X-ray absorption, they can be considered as being equivalent to water of a higher density. In Fig. 3.9, it is shown how material decomposition into iodine and water can be used to calculate the iodine enhancement and virtual non-contrast images based on a simple parallel projection in the CT-value diagram (Fig. 3.9).

With a dual-energy post-processing algorithm, based on the three-material decomposition principle, iodine can be subtracted or overlaid on conventional gray-scale information, and therefore, a iodine spectral-extraction series, consisting of virtual unenhanced and color-coded iodine overlay images, is achieved

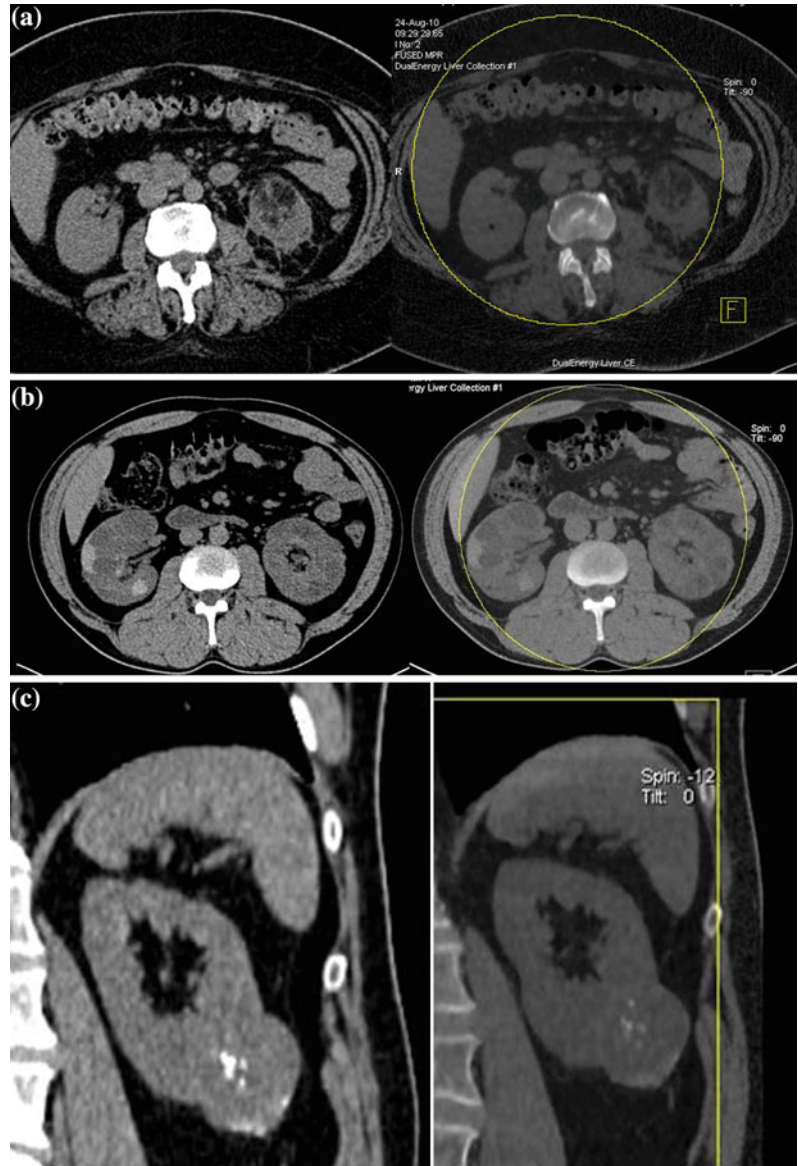
(Fig. 3.8) [39–41]. If the technology and scanning techniques are optimized, the necessity for a baseline-unenhanced CT acquisition could be eliminated, leading to significant reductions in radiation dose to patients.

The evaluation of cystic and solid renal masses represents one of most investigated applications of dual-energy CT technology [43, 44, 51, 52, 54, 55]. Similar to current single-energy CT imaging evaluation of a mass, the virtual-unenhanced images can be used to replace the true unenhanced CT acquisition. The attenuation of the lesion on the virtual-unenhanced series can serve as a baseline to compare with the contrast-enhanced series. Several studies [53, 54, 56] demonstrated that no significant difference in the attenuation of renal lesions between true and virtual unenhanced images exists (Fig. 3.10).

The possibility of omitting the true unenhanced scan permits to achieve a considerable radiation dose saving in renal lesions imaging [52, 53, 57].

Compared with a standard triple phase single-energy MDCT protocol, Graser et al. [53] found a 35 % radiation dose decrease if a dual-energy dual-phase protocol, with subsequent reconstruction of virtual unenhanced images, is carried out. The same author showed that it is possible to dramatically cut the patient radiation exposure up to 50 % whether a single-phase MDCT protocol is performed [52]. The radiation dose saving achievable with the use of virtual unenhanced images represents a considerable advantage in patients with complex cystic renal lesions because many of these patients need follow-up for many years. A recent study demonstrated that, in the specific clinical setting of complex cystic renal masses, dual-energy CT permits to achieve a mean dose reduction of 29 % while being able to show all possible attenuation features present in renal cyst, including liquid low-attenuation (due to liquid or necrosis), intermediate-attenuation (due to soft-tissue solid nodule or debris), high-attenuation (due to hemorrhage or protein-rich content) and calcification (Fig. 3.10) [54].

**Fig. 3.10** Examples of virtual unenhanced with corresponding true unenhanced image series in lipid-rich angiomyolipoma of the left kidney (a), perinephric right hematoma due to hemorrhagic cyst bleeding (b), and solid RCC of the left kidney showing huge calcification (c). Note that the two image series can be easily discriminated, since virtual unenhanced images appear slightly grainier than conventional unenhanced series due to the lower kVp and smoothing induced by the post-processing algorithm. Note also the yellow ring which corresponds to the field-of-view on the tube with the smaller detector (26 cm)



Dual-energy color-coded iodine overlay images permit to immediately depict the presence of contrast medium within a mass by means of a color display. With this method, one can immediately perceive visual enhancement in a mass not relying on measured changes in attenuation (Figs. 3.11, 3.12). The direct visualization of iodine signal within the mass differentiates a cyst from a solid lesion. As renal cysts do not contain blood vessels centrally, color-coded iodine overlay image shows a cyst as devoid of iodine

signal. In contrast, solid renal masses do have vessels within them, and these vessels and the tissue of the mass accumulate iodine after contrast injection. Brown first described this possible use of dual-energy CT in phantom studies, founding color-coded iodine overlay technique highly sensitive in identification of enhancing renal masses [44]. The clinical use of iodine-specific images has since been reported as well [52, 54, 57–59]. Furthermore, as found by Graser, use of a color-coded iodine overlay reduces

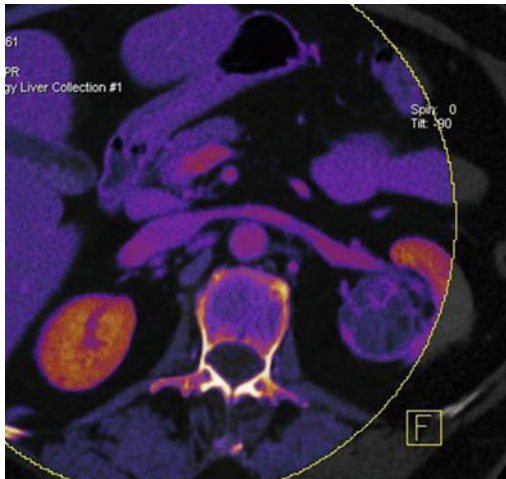


**Fig. 3.11** Axial color-coded iodine overlay image in a patient with multilocular cystic left RCC. Note that the solid enhancing nodules within the tumor show iodine uptake displayed as color-coded signal, whereas the cystic areas are displayed as signal void

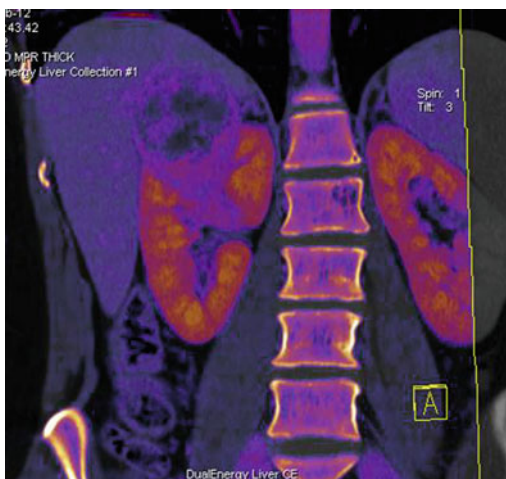


**Fig. 3.12** Coronally reformatted color-coded iodine overlay image in a patient with right kidney RCC. Note that the healthy enhancing renal parenchyma as well as solid enhancing nodules within the tumor shows iodine uptake displayed as color-coded signal. Note that necrotic areas are displayed as signal void

post-processing time because enhancement can be directly quantified with the overlay function available in the dual-source dual-energy CT system, eliminating the need for double-ROI

measurements and calculation of attenuation change on two images [53]. Therefore, this technique permits to overcome some problems related to multiphase acquisition. However, this technique does not permit to address the problem of equivocal enhancement, especially in demonstrating low-level true enhancement in solid enhancing lesions (Fig. 3.13).

Overall, at dual-energy CT, there are two different ways to quantify the iodine uptake of a lesion. Firstly, it is possible to measure the iodine enhancement of the lesion, similar to the comparison of unenhanced and contrast-enhanced images with single-energy CT. As an alternative approach independent of attenuation measurement, the lesion iodine concentration (in mg/mL) can be calculated. This approach provides a more direct measure of lesion vascularity (Fig. 3.14).

Chandarana [59] found that iodine quantification with dual-energy CT is accurate in a phantom model and that the presence of an iodine concentration greater than 0.5 mg/mL in a renal lesion was equivalent to the diagnosis of enhancement on basal and contrast-enhanced acquisitions. The author supposed that qualitative or quantitative depiction of iodine may be superior to attenuation measurements, especially in discriminating minimally enhancing tumors, such as papillary subtypes of renal cancer, from high-attenuation cysts [59].

Recently, Ascenti et al. [60] demonstrated that spectral-based dual-energy CT iodine quantification is more accurate than standard enhancement measurements in distinguishing enhancing from non-enhancing renal masses, especially in depicting minimally enhancing neoplasms, such as papillary RCC and/or in excluding enhancement in small renal cysts (Figs. 3.15 and 3.16).

Kaza et al. [43] using a single-source fast-kilovoltage switching dual-energy CT reported a series of 83 renal lesions. These authors found that a measured iodine density threshold of 2 mg/cm<sup>3</sup> had the highest accuracy (92.8 %) in detecting enhancing renal masses with a sensitivity of 90 % and specificity of 93 %.

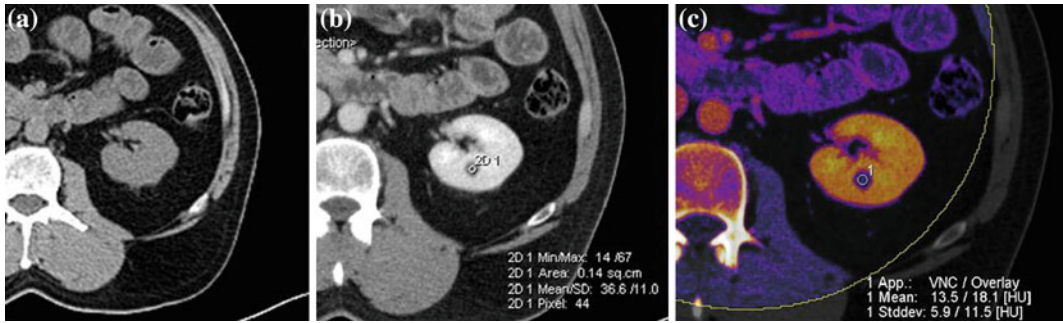


**Fig. 3.13** Small left intra-renal simple cyst. **a** unenhanced single energy; **b** contrast-enhanced nephrographic phase dual-energy linear-blended (M 0.3); **c** contrast-enhanced nephrographic phase dual-energy color-coded iodine overlay. The small hypodense intrarenal lesion is visible only in nephrographic phase; **(b)** the delta of

attenuation cannot be accurately evaluated in conventional imaging. Whereas dual-energy evaluation demonstrated a virtual basal attenuation of 13 HU, the enhancement of lesion remain equivocal. The attenuation increase of 18 HU is more probably due to pseudoenhancement, though a small hypovascular tumor cannot be excluded



**Fig. 3.14** Coronally-reformatted color-coded iodine overlay image in a patient having RCC, clear cell type, and simple cyst of the right kidney. Note that RCC shows iodine uptake, expressed by a single ROI as iodine-based enhancement (*Overlay*) and iodine concentration (in mg/mL); conversely, simple cyst does not show any iodine uptake

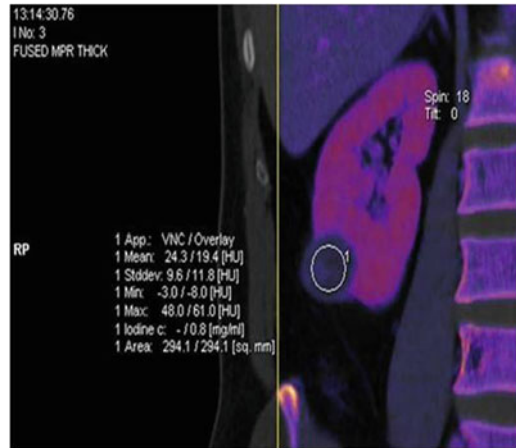


**Fig. 3.15** Coronally reformatted color-coded iodine overlay image in a patient with RCC, clear cell type, of the right kidney. Note that while the lesion shows borderline attenuation-based enhancement, an evident iodine uptake is seen whether the iodine concentration is considered

Therefore, these differences in the cutoff point value reported between the two main hardware platforms need to be explained and further investigated.

More recently, Liu et al., showed that D-value (defined as the absolute difference between the CT value at 80 and 140 kVp images) and dual-energy ratio (called as CT value with 80 kV divided by the value with 140 kV) indexes are

useful parameters for distinguishing homogeneously high-attenuation renal cysts from enhancing solid renal masses using a single phase dual-energy MDCT protocol. A D-value of 17.6 HU and a dual-energy ratio of 1.3 were found as most accurate cutoff point for enhancement detection [61]. Similar results were previously reported in a phantom experiment using a second-generation dual-source system [62].

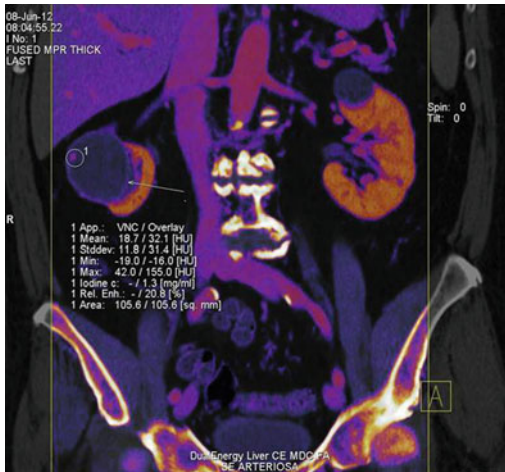


**Fig. 3.16** Coronally reformatted color-coded iodine overlay image in a patient having a right kidney complex cyst and left kidney simple cyst. Note the enhancing irregular thick wall (*arrow*) and the enhancing nodule (ROI) of the neoplastic complex cyst. The absence of vascularization of the simple left cyst is seen

Finally, iodine quantification in dual-energy CT seems to have a potential to reduce renal pseudoenhancement of small simple or hyperattenuating cysts (Figs. 3.17 and 3.18).

Based on material decomposition and the knowledge of mass attenuation of materials, dual-energy enables *energy-specific* application, represented by the creation of virtual monochromatic images. In particular, a mathematic computerized model is applied to the polychromatic source data obtained from the dual-energy acquisition. However, whether a single-source fast-kVp switching platform is used, monochromatic images are synthesized in the data domain, whereas for dual-energy CT, data acquired with dual-source CT systems, image domain basis material decomposition is typically used. This is due to the fact that projection data deriving from the low- and high-energy scans are collected by the dual-source system in helical mode, and thus, data are not coincident one with each other. For a given photon energy, virtual monochromatic images, whose energy is reported as kiloelectronvolts (keV) instead of peak voltage (kVp),

mimic those images that would result from a true monochromatic X-ray source. The advantage of a monochromatic beam is that it is less susceptible to beam-hardening artifact and therefore has the potential to provide more accurate and more reproducible attenuation measurements over conventional MDCT. Preliminary experiences show that monochromatic images permit to alleviate the pseudoenhancement phenomenon in renal cysts [63]. Similar results are obtained in a phantom study using a second-generation dual-source system [64].

Furthermore, with the use of dedicated software applications, keV spectral attenuation curves can be generated by plotting the attenuation values (in HU) of a material at different monochromatic energies, ranging from 40 to 140 keV. With this technique, specific tissue characterization is achievable based on known mean attenuation characteristics of different materials, especially those with higher atomic numbers, enhancing solid renal lesions may be therefore differentiated from non-enhancing cysts in a single-phase nephrographic image on the basis of the attenuation curves (Fig. 3.19) [65, 66]. In particular, iodine-containing lesions show an upwardly steep curve at the decrease of energy levels, whereas avascular cysts show relatively flat curves at all energies; these curves can be also normalized using the healthy renal parenchyma as reference background. By indirectly identifying the iodine uptake, this method may also open new perspective to assess response to therapy and tumor viability.

Overall, the choice of study phase for the dual-energy scan is the first step, and it depends on the specific clinical scenario. If a renal mass (e.g., previously detected by US examination) has to be characterized the best CT phase for performing the dual-energy scan is the nephrographic phase. In this setting, all advantages of dual-energy CT images in the enhancement analysis can be exploited. Conversely, whether a patient with a known renal mass undergoes CT for staging, the opportunity of performing the dual-energy scan during the corticomedullary





**Fig. 3.17** Standard 120-kVp (*on the left*) and corresponding dual-energy color-coded iodine overlay (*on the right*) images of a phantom containing a vial of water immersed in an iodine solution (20 mg/mL). The lower ROI on the standard 120-kVp image clearly demonstrates

pseudoenhancement, whereas the ROI at the corresponding level on DE image shows no surreptitious elevation of attenuation. Iodine quantification in mg/mL confirms the absence of iodine into the vial (−0.2 mg/mL)

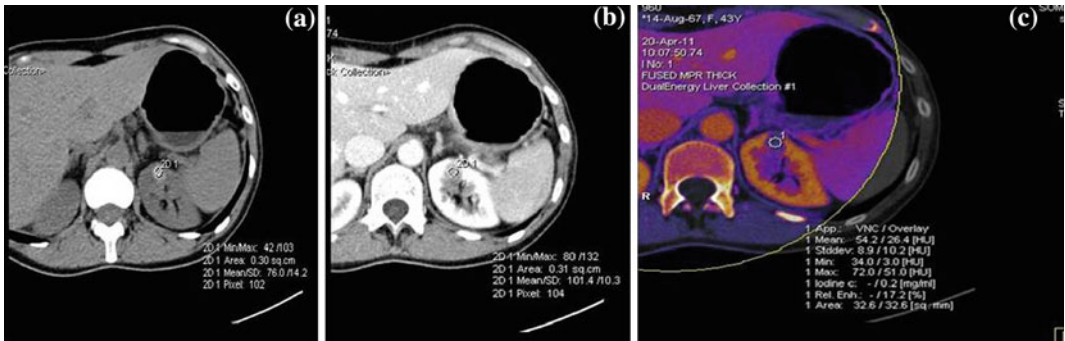


**Fig. 3.18** Small hyperdense intraparenchymal left renal cyst showing pseudoenhancement at conventional CT evaluation. Axial CT images. **a** unenhanced single-energy phase; **b** contrast-enhanced nephrographic phase dual-energy linear-blended (M 0.3); **c** contrast-enhanced nephrographic phase dual energy with color-coded iodine

overlay. The basal attenuation of the cyst (76 HU) increased of 25 HU mimicking enhancement of a solid lesion. In such case, a renal tumor as a papillary carcinoma cannot be excluded. Diagnosis of hyperdense cyst is confidently made for the absence of iodine into the lesion (0.2 mg/mL)

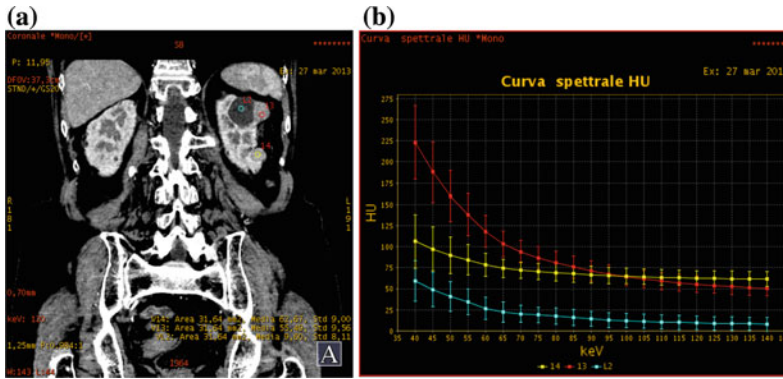


**Fig. 3.19** Renal cell carcinoma, simple and high-attenuation left renal cyst. **a** Monochromatic DECT image (120 keV) shows a hypoattenuating left renal lesion (*light blue ROI*) and two hyperattenuating left renal lesions (*red and yellow ROI*). The first lesion is likely to be a cyst (attenuation < 10 HU). The remaining two lesions have an indeterminate appearance that could represent either an enhancing mass or a high-attenuation cyst. **b** the graphic shows DECT spectral attenuation

curves for the three lesions at various kiloelectron-volt values. The hypodense (*light blue ROI*) and one high-attenuation (*yellow ROI*) lesions have flat curves, indicating that they are avascular. The first is a simple cyst and the latter is a hemorrhagic or a proteinaceous cyst. The remaining hyperdense left renal lesion (*red ROI*) is an enhancing mass and it has a more steeply increasing slope at lower energies. (Courtesy of Prof. Luca Volterrani, Department of Radiology University of Siena, Italy)

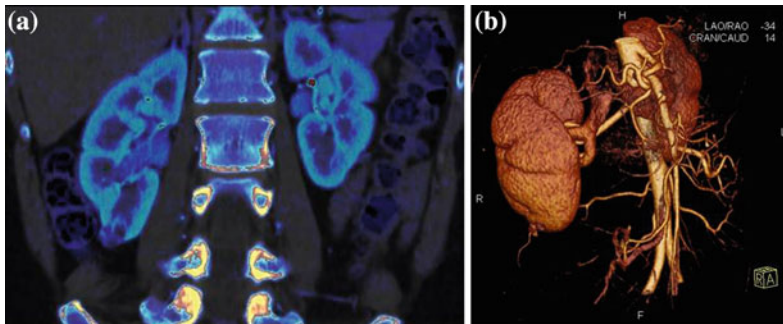


**Fig. 3.20** Small cystic hypervascular renal cell carcinoma of the lower right kidney pole suitable for nephron-sparing surgery. Coronally reformatted dual-energy color-coded iodine overlay CT image during cortico-medullary phase (**a**) and Volume Rendering image after

dual-energy bone removal (**b**) show an accessory artery for the right lower pole and a large vein draining the tumor, both representing useful information for the surgeon



**Fig. 3.21** Dual-energy linear-blended axial CT image during cortico-medullary phase (a) shows a small hypovascular left renal cell carcinoma in a patient with right nephrectomy. (b) MIP coronal CT image and (c) MIP coronal CT image after dual-energy bone removal.

The presence of three left renal arteries, well demonstrated after bone removal (*arrows*), represents very useful pre-surgical information when a nephron-sparing surgery is expected

phase should be considered. By taking advantage of greater iodine conspicuity at 80 kVp and automated bone subtraction with the dual-energy software, effective 3D reconstruction of the renal vascular map, which are required for pre-surgical urologic planning, can be rapidly achieved (Figs. 3.20 and 3.21). The coverage of the dual-energy CT scan varies from hepatic dome to iliac crest for the corticomedullary phase, whereas from hepatic dome to pubic symphysis for the nephrographic phase.

## References

1. Tada S, Yamagishi J, Kobayashi H et al (1983) The incidence of simple renal cysts by computed tomography. *Clin Radiol* 34:437–439
2. Jayson M, Sanders H (1998) Increased incidence of serendipitously discovered renal cell carcinoma. *Urology* 51:203
3. Konnak JW, Grossman HB (1985) Renal cell carcinoma as an incidental finding. *J Urol* 134:1094–1096
4. Luciani LG, Cestari R, Tallarigo C (2000) Incidental renal cell carcinoma—age and stage characterization and clinical implications: study of 1092 patients (1982–1997). *Urology* 56:58–62
5. Israel GM, Bosniak MA (2005) How I do it: evaluating renal masses. *Radiology* 236:441–450
6. Siegel R, Ward E, Brawley O et al (2011) Cancer statistics, 2011. *CA Cancer J Clin* 61:212–236
7. Lopez-Beltran A, Scarpelli M, Montironi R et al (2006) 2004 WHO Classification of the Renal Tumors of the Adults. *Eur Urol* 49:798–805
8. Grignon DJ, Che M (2005) Clear cell renal cell carcinoma. *Clin Lab Med* 25:305–316
9. Eble JN, Sauter G, Epstein JI et al (2004) Pathology and genetics. Tumors of the urinary system and male genital organs. IARC Press, Lyon
10. Brunelli M, Eble JN, Zhang S et al (2005) Eosinophilic and classic chromophobe renal cell carcinomas have similar frequent losses of multiple chromosomes from among chromosomes 1, 2, 6, 10, and 17, and this pattern of genetic abnormality is not present in renal oncocytoma. *Mod Pathol* 18: 161–169
11. Mostofi FK, Davis CJ (1998) Histological typing of kidney tumors. Springer, Berlin
12. Wagner BJ, Wong-You-Cheong JJ, Davis CJ Jr (1997) Adult renal Hamartomas. *Radiographics* 17:155–169
13. Bosniak MA (1986) The current radiological approach to renal cysts. *Radiology* 158:1–10
14. Harisinghani MG, Maher MM, Gervais DA (2003) Incidence of Malignancy in Complex Cystic Renal Masses (Bosniak Category III): Should Imaging-Guided Biopsy Precede Surgery? *AJR* 180: 755–758
15. Sauk SC, Hsu MS, Margolis DJ et al (2011) Clear cell renal cell carcinoma: multiphasic multidetector CT imaging features help predict genetic karyotypes. *Radiology* 261:854–862
16. Israel GM, Bosniak MA (2008) Pitfalls in Renal Mass Evaluation and How to Avoid Them. *Radiographics* 28:1325–1338
17. Birnbaum BA, Jacobs JE, Ramchandani P (1996) Multiphasic renal CT: comparison of renal mass enhancement during the corticomedullary and nephrographic phases. *Radiology* 200:753–758
18. Cohan RH, Sherman LS, Korobkin M et al (1995) Renal masses: assessment of corticomedullary-phase and nephrographic-phase CT scans. *Radiology* 196:445–451

19. Herts BR, Coll DM, Novick AC et al (2002) Enhancement characteristics of papillary renal neoplasms revealed on triphasic helical CT of the kidneys. *AJR Am J Roentgenol* 178:367–372
20. Israel GM, Silverman SG (2011) The incidental renal mass. *Radiol Clin N Am* 49:369–383
21. Bosniak MA (1997) Diagnosis and management of patients with complicated cystic lesions of the kidney. *AJR Am J Roentgenol* 169:819–821
22. Israel GM, Bosniak MA (2003) Follow-up CT of moderately complex cystic lesions of the kidney (Bosniak category IIF). *AJR Am J Roentgenol* 181:627–633
23. Israel GM, Bosniak MA (2003) Calcification in cystic renal masses: is it important in diagnosis? *Radiology* 226:47–52
24. Bosniak MA (1997) The use of the Bosniak classification system for renal cysts and cystic tumors. *J Urol* 157:1852–1853
25. Bosniak MA (1991) Difficulties in classifying cystic lesion of the kidney. *Urol Radiol* 13:91–93
26. Bosniak MA (1993) Problems in the radiologic diagnosis of renal parenchymal tumors. *Urol Clin North Am* 20:217–230
27. Bosniak MA (1991) The small (less than or equal to 3.0 cm) renal parenchymal tumor: detection, diagnosis, and controversies. *Radiology* 179:307–317
28. Hartman DS, Davis CJ, Johns T et al (1986) Cystic renal cell carcinoma. *Urology* 28:145–153
29. Murad T, Komaiko W, Oyasu R et al (1991) Multilocular cystic renal cell carcinoma. *Am J Clin Pathol* 95:633–637
30. Bosniak MA (1996) Cystic renal masses: a reevaluation of the usefulness of the Bosniak Classification System (letter). *Acad Radiol* 3:981–984
31. Silverman SG, Israel GM, Herts BR et al (2008) Management of the incidental renal mass. *Radiology* 249:16–31
32. McGahan JP, Lamba R, Fisher J et al (2011) Is Segmental Enhancement Inversion on Enhanced Biphasic MDCT a Reliable Sign for the Noninvasive Diagnosis of Renal Oncocytomas? *AJR Am J Roentgenol* 197:W674–W679
33. Millet I, Curros Doyon F, Hoa D et al (2011) Characterization of Small Solid Renal Lesions: Can Benign and Malignant Tumors Be Differentiated With CT? *AJR Am J Roentgenol* 197:887–896
34. Bosniak MA, Megibow AJ, Hulnick DH et al (1988) CT diagnosis of renal angiomyolipoma: the importance of detecting small amounts of fat. *AJR Am J Roentgenol* 151:497–501
35. Inzaki M, Tanimoto A, Narimatsu Y et al (1997) Angiomyolipoma: imaging findings in lesions with minimal fat. *Radiology* 205:497–502
36. Birnbaum BA, Hindman N, Lee J et al (2007) Renal cyst pseudoenhancement: influence of multidetector CT reconstruction algorithm and scanner type in phantom model. *Radiology* 244:767–775
37. Maki DD, Birnbaum BA, Chakraborty DP et al (1999) Renal cyst pseudoenhancement: beam-hardening effects on CT numbers. *Radiology* 213:468–472
38. Fornaro J, Leschka S, Hibbeln D et al (2011) Dual- and multi-energy CT: approach to functional imaging. *Insights imaging* 2:149–159
39. Johnson TR, Krauss B, Sedlmair M et al (2007) Material differentiation by dual energy CT: initial experience. *Eur Radiol* 17:1510–1517
40. Petersilka M, Bruder H, Krauss B et al (2008) Technical principles of dual source CT. *Eur J Radiol* 68:362–368
41. Graser A, Johnson TR, Chandarana H et al (2009) Dual energy CT: preliminary observations and potential clinical applications in the abdomen. *Eur Radiol* 19:13–23
42. Fletcher JG, Takahashi N, Hartman R et al (2009) Dual-energy and dual-source CT: is there a role in the abdomen and pelvis? *Radiol Clin North Am* 47:41–57
43. Kaza R, Caoili EM, Cohan RH et al (2011) Distinguishing enhancing from nonenhancing renal lesions with fast kilovoltageswitching dual-energy CT. *AJR Am J Roentgenol* 197:1375–1381
44. Brown CL, Hartman RP, Dzyubak OP et al (2009) Dual-energy CT iodine overlay technique for characterization of renal masses as cyst or solid: a phantom feasibility study. *Eur Radiol* 19: 1289–1295
45. Megibow AJ, Sahani D (2012) Best practice: implementation and use of abdominal dual-energy CT in routine patient care. *AJR Am J Roentgenol* 199:S71–S77
46. Eusemann C, Holmes DR III, Schmidt B (2008) Dual energy CT: how the best blend both energies in one fused image? *SPIE 6918 Medical imaging*, San Diego
47. Kim KS, Lee JM, Kim SH et al (2010) Image fusion in dual energy computed tomography for detection of hypervascular liver hepatocellular carcinoma: phantom and preliminary studies. *Invest Radiol* 45:149–157
48. Yu L, Primak AN, Liu X et al (2009) Image quality optimization and evaluation of linearly mixed images in dual-source, dual-energy CT. *Med Phys* 36:1019–1024
49. Holmes DR, 3rd, Fletcher JG, Apel A, et al. (2008) Evaluation of non-linear blending in dual-energy computed tomography. *Eur J Radiol* 68:409–413
50. Apel A, Fletcher JG, Fidler JL et al (2011) Pilot multi-reader study demonstrating potential for dose reduction in dual energy hepatic CT using non linear blending of mixed kV image datasets. *Eur Radiol* 21:644–652
51. Ascenti G, Krauss B, Mazziotti S et al (2012) Dual-energy computed tomography (DECT) in renal masses: nonlinear versus linear blending. *Acad Radiol* 19:1186–1193
52. Graser A, Becker CR, Staehler M et al (2010) Single-phase dual-energy CT allows for characterization of renal masses as benign or malignant. *Invest Radiol* 45:399–405

53. Graser A, Johnson TR, Hecht EM et al (2009) Dual-energy CT in patients suspected of having renal masses: can virtual nonenhanced images replace true nonenhanced images? *Radiology* 252:433–440
54. Ascenti G, Mazziotti S, Mileto A et al (2012) Dual-source dual-energy CT evaluation of complex cystic renal masses. *AJR Am J Roentgenol* 199:1026–1034
55. Heye T, Nelson RC, Ho LM et al (2012) Dual-energy CT applications in the abdomen. *AJR Am J Roentgenol* 199:S64–S70
56. Neville AM, Gupta RT, Miller CM et al (2011) Detection of renal lesion enhancement with dual-energy multidetector CT. *Radiology* 259:173–183
57. Ascenti G, Mileto A, Gaeta M et al (2013) Single-phase dual-energy CT urography in the evaluation of haematuria. *Clin Radiol* 68:87–94
58. Kang SK, Kim D, Chandarana H (2011) Contemporary imaging of the renal mass. *Curr Urol Rep* 12:11–17
59. Chandarana H, Megibow AJ, Cohen BA et al (2011) Iodine quantification with dual-energy CT: phantom study and preliminary experience with renal masses. *AJR Am J Roentgenol* 196:693–700
60. Ascenti G, Mileto A, Krauss B, et al. (2013) Distinguishing enhancing from nonenhancing renal masses with dual-source dual-energy CT: iodine quantification versus standard enhancement measurements. *Eur Radiol* doi:10.1007/s0030-013-2811-4
61. Liu XL, Zhou JJ, Zeng MS et al (2013) Homogeneous high attenuation renal cysts and solid masses—differentiation with single phase dual energy computed tomography. *Clin Radiol* 68:198–205
62. Karlo C, Lauber A, Gotti RP et al (2011) Dual-energy CT with tin filter technology for the discrimination of renal lesion proxies containing blood, protein, and contrast-agent. An experimental phantom study. *Eur Radiol* 21:385–392
63. Jung DC, Oh YT, Kim MD et al (2012) Usefulness of the virtual monochromatic image in dual-energy spectral CT for decreasing renal cyst pseudoenhancement: a phantom study. *AJR Am J Roentgenol* 199:1316–1319
64. Yamada S, Ueguchi T, Ukai I et al (2012) The potential of dual-energy virtual monochromatic imaging in reducing renal cyst pseudoenhancement: a phantom study. *Nihon Hoshasen Gijutsu Gakkai Zasshi* 68:1379–1384
65. Yu L, Leng S, McCollough CH (2012) Dual-energy CT-based monochromatic imaging. *AJR Am J Roentgenol* 199:S9–S15
66. Silva AC, Morse BG, Hara AK et al (2011) Dual-energy (spectral) CT: applications in abdominal imaging. *Radiographics* 31:1031–1046